Optoacoustic endoscopy in curved scanning mode

Hailong He [a,b], Andreas Buehler [a,b*], and Vasilis Ntziachristos [a,b]

[a] *Institute for Biological and Medical Imaging, Helmholtz Zentrum München, Ingoldstädter Landstraße 1, 85764 Neuherberg, Germany*
[b] *Chair for Biological Imaging, Technische Universität München, Ismaninger Str. 22, 81675 München, Germany*

ABSTRACT

Optoacoustic technique has been shown to resolve anatomical, functional and molecular features at depths that go beyond the reach of epi-illumination optical microscopy offering new opportunities for endoscopic imaging. Herein, we interrogate the merits of optoacoustic endoscopy implemented by translating a sound detector in linear or curved geometries. The linear and curved detection geometries are achieved by employing an intravascular ultrasound transducer (IVUS) within a plastic guide shaped to a line or a curve. This concept could be used together with optical endoscopes to yield hybrid optical and optoacoustic imaging.

Keywords: Optoacoustic imaging, optoacoustic tomography imaging, curved scanning geometry

1. INTRODUCTION

White-light endoscopy is a common optical imaging medical procedure employed to visualize tissues and disease inside the human body but comes with two important limitations. First, it attains access only to superficial tissues since it is not possible to visualize under the tissue surface. Second, endoscopic detection is based on superficial architectural features and tissue discoloration, which is not always very specific. To increase contrast and disease detection specificity, different optical methods have been considered as an addition to white-light imaging. For example, narrow-band imaging [1], endoscopic optical coherence tomography [2] and confocal laser endoscopy [3] have been clinically applied, but are not yet selected for mainstream use. In all cases however, due to the use of an all-optical method, scattering brings important limitations to the resolution and depth that can be achieved.

Endoscopic ultrasound achieves penetration of several millimeters to centimeters in tissue and thus can provide information about subsurface morphology such as displacia [4]. However, by relying on the bulk mechanical properties of tissue, endosonography only provides weak soft tissue contrast, low sensitivity and no physiologically specific functional information.

To improve on these limitations, optoacoustic imaging has been proposed for endoscopy [5], as it can retain the penetration depth and resolution of ultrasound but provides rich optical contrast. Optoacoustic contrast is significantly enhanced via the application of multispectral optoacoustic tomography (MSOT) [6]. The technique illuminates tissues at multiple wavelengths and can offer specific detection of tissue chromophores and administered optical agents by detecting their absorption spectrum over the background absorption [6].

Optoacoustic endoscopy has been so far implemented using dedicated endoscopes operating on rotational and linear translational scanning of ultrasound sensors yielding cross-sectional B-scan images [7-9]. Implementations of this concept have been presented using single-element unfocused [8] and focused [7] detectors.

Herein, we present curved scanning optoacoustic endoscopy[10]. The curved geometry offers larger effective acceptance aperture than the linear translation approach and thus helps to improve image quality by capturing a larger fraction of the ultrasound field emitted from tissue. We implemented both the curved and the traditional linear scanning approaches and compared them by imaging phantoms and tumor mice in-vivo.

Photons Plus Ultrasound: Imaging and Sensing 2016, edited by Alexander A. Oraevsky, Lihong V. Wang
Proc. of SPIE Vol. 9708, 97080J · © 2016 SPIE · CCC code: 1605-7422/16/$18 · doi: 10.1117/12.2210962

2. MATERIALS AND METHOD

2.1 Endoscopic imaging configuration

Fig. 1 depicts the schematic of the endoscopy system and a photograph of the distal end of the proposed curved optoacoustic tomography endoscopy probe respectively. A commercial IVUS sensor (2.5-Fr, Atlantis SR Pro, Boston Scientific, Natick, MA) with a center frequency 15 MHz was used for signal detection. The active element of the sensor had a disc-like shape with a diameter of 0.8 mm yielding an acceptance angle of 30 degrees as derived experimentally from point-source measurements. The transducer was inserted in the bigger lumen of a two-lumen flexible polyethylene terephthalate (PET) tube (Boston Scientific, USA) with an outer diameter of 2.5 mm. The transducer could be translated within the lumen using a proximal translation stage. A curved metal wire (0.5 mm in diameter) was inserted into the second lumen of the tube to give the tube a specific shape. This defined the curved scanning geometry. The tube was cut open at the sensing side of the transducer over a length of 4 cm to improve propagation of sound. For illumination we used a nanosecond pulsed laser (Phocus, Opotek USA). The illumination wavelength was 700nm. A fiber bundle was used to guide laser light onto the sample. The light fluence at the surface of the sample was 18 mJ/cm2. The detected acoustic signals were amplified by 63dB (AU-1291, Mited Inc., Haupppauge, New York, USA) and recorded with the data acquisition card (CS122G1, Gage, Lockport, Illinois, USA; 12-bit resolution; max sampling rate, 2GS/S).

Two imaging configurations were investigated, i.e. a linear geometry with the ultrasound element scanned along a straight line and a curved geometry with the ultrasound element scanned over a 90 degrees arc with a radius of 22.6 mm as shown in Fig. 1 (b). The scanning length was 36 mm in both cases and data from 200 consecutive scanning positions averaged over 5 laser pulses was acquired. The signals measured were first deconvolved with the electrical impulse response of the system and bandpass filtered between 1-20 MHz. Then image reconstruction was performed using back-projection [11]. Negative values resulting from experimental inaccuracies and the use of an approximate inversion scheme were set to zero because they do not have any physical meaning.

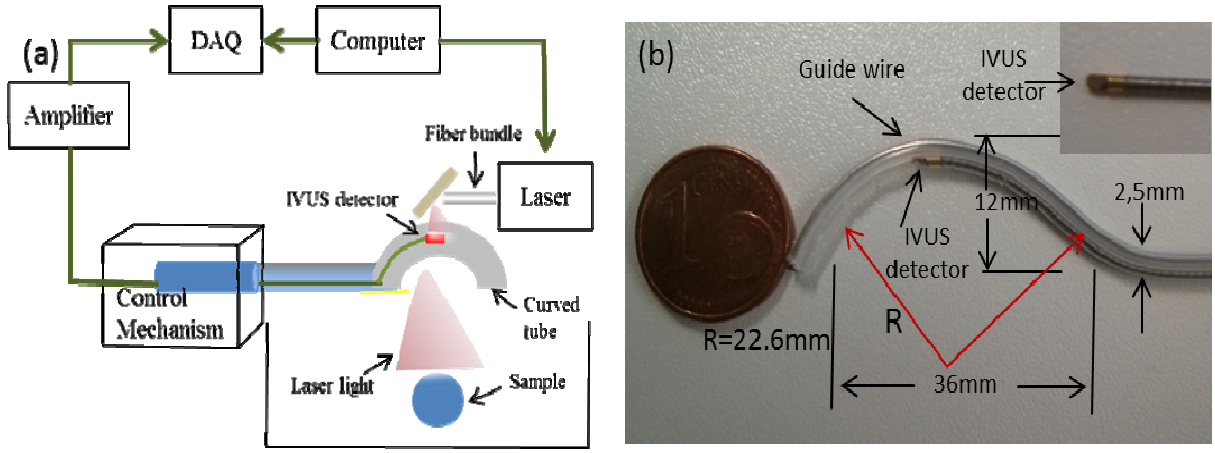

Fig. 1. (a) Schematic illustration of the imaging setup; (b) photograph of the distal end of the curved endoscopy probe.

2.2 Phantom and tissue measurements

To characterize the imaging performance of the system under defined conditions, two phantoms were imaged: First, a microsphere phantom consisting of several black polyethylene microspheres with an approximate diameter of 200 µm (Cospheric BKPMS 180−210 µm). Second a 2D phantom built by printing a complex pattern on a sheet of paper using a laser printer (FS-C5400DN). All samples where embedded in a transparent 1.9cm in diameter agar cylinder made of 2%w/v agar (Sigma, Germany). Water was used as a coupling medium to propagate the acoustic waves from the sample to the detector. To examine the performance of the two approaches on tissue data, we imaged a four-week-old athymic nude-Foxn1nu mouse with a 4T1 subcutaneous tumor. All procedures were approved by the District Government of Upper Bavaria. The mouse was anesthetized

under 1.8% isoflurane anesthesia. Sound coupling was achieved using a water bed where the tumor was immersed, whereby the mouse was kept outside the water and its body temperature was maintained at 36 °C. After the measurements, the mouse was sacrificed and cryosliced in cross-sections parallel to the imaging plane.

3. RESULTS

Fig. 2 presents the optoacoustic images of microsphere phantom imaged in the linear and curved scanning geometry. Images obtained with the linear geometry (Fig. 2b) and curved geometry [Fig. 2(c)] reveal the imaging ability of the two implementations. The result of linear scanning showcases, as expected, a lateral elongation of the reconstructed microspheres. The image also contains some visible artifacts. Conversely, the image obtained by the curved geometry exhibits better definition of the actual size and shape of the spheres and reduces the appearance of artifacts. Fig. 2(d) shows the profiles obtained through the images of the microspheres along the direction of detector translation and confirm a significant improvement of lateral resolution. For example, the resolution characterized as the full width at half-maximum (FWHM) along the lateral direction of microsphere 3 is improved from 520 um in linear mode to 207 um in curved mode, the latter value representing the true size of the sphere.

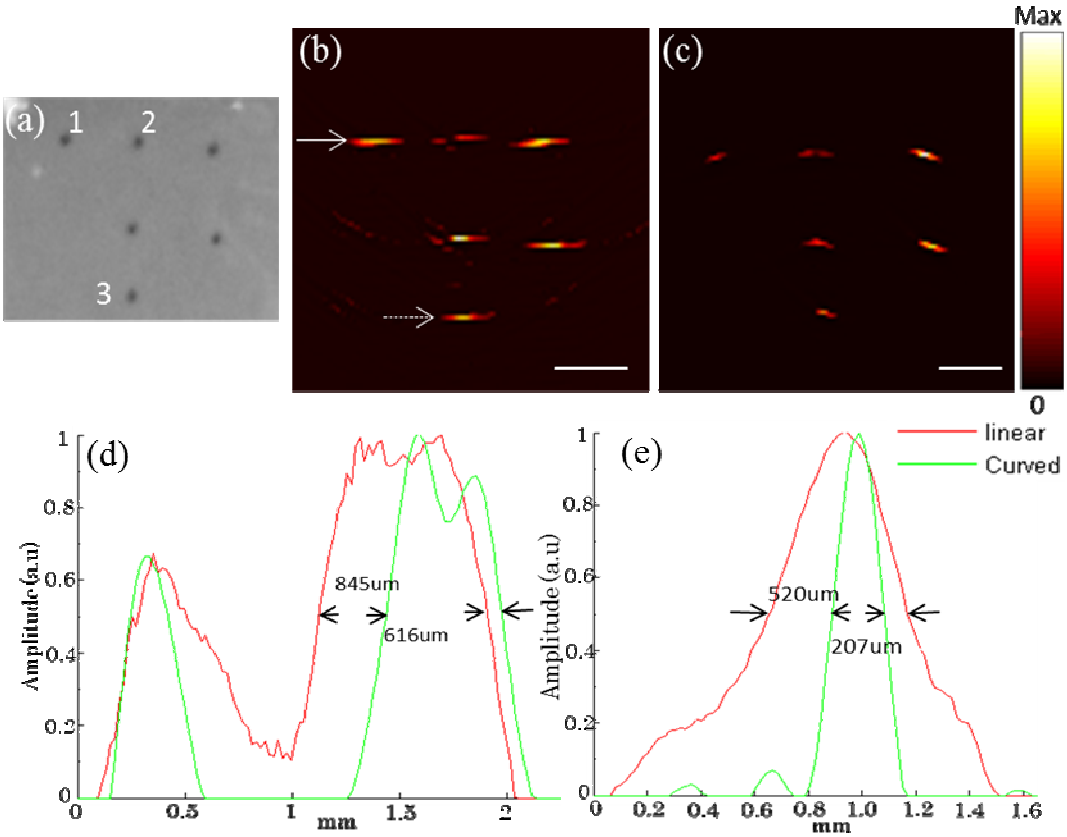

Fig. 2. (a) Photograph of the microsphere phantom. (b) shows the result in the linear geometry and (c) in the curved geometry. (d) shows the lateral profile (the white arrow) thorough microsphere 1 and 2, respectively and (e) the profile through microsphere 3 (the white dash arrow). Scalebar 1 mm.

An illustration of the 2D phantom is shown in Fig. 3(a). Reconstructed results of linear and curved configurations are then shown on Fig. 3(b) and 3(c), respectively. In analogy to the microsphere phantom, the reconstruction in the curved geometry better resolves the absorbing features of the phantom and shows fewer artifacts compared to the results obtained in the linear geometry. Fig. 3(c) correctly captures the size of the big

circles measuring double the diameter of the small circles as printed on the phantom. However in the linear mode, those features are hardly resolved and the big circles cannot be clearly identified as circular objected on Fig. 3(b). The shape of all objects is better resolved and appears more continuous in the curved scan than in the linear scan.

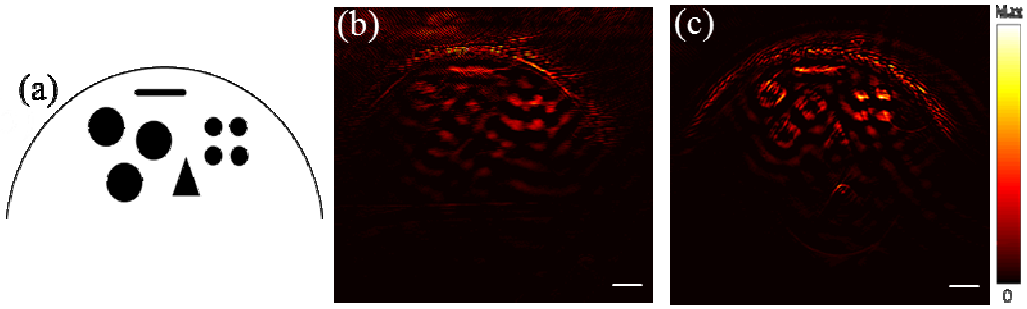

Fig. 3. (a) Illustration of the pattern printed onto the paper phantom. Reconstruction results in the linear (b) and curved (c) mode. Scalebar 1 mm.

Fig. 4 presents the results of the tumor measurement in the linear and curved modes. Fig. 4(a) shows a photograph of the cryoslice approximately corresponding to the imaging plane. The corresponding reconstructions of the linear and curved modes are presented in Fig. 4(b) and 4(c). The tumor boundaries are resolved with higher contrast and less artifacts in the curved imaging mode, compared to the linear mode. The overall resolution achieved is also better in curved scanning mode, as evident in the insets of Fig. 4(b) and 4(c).

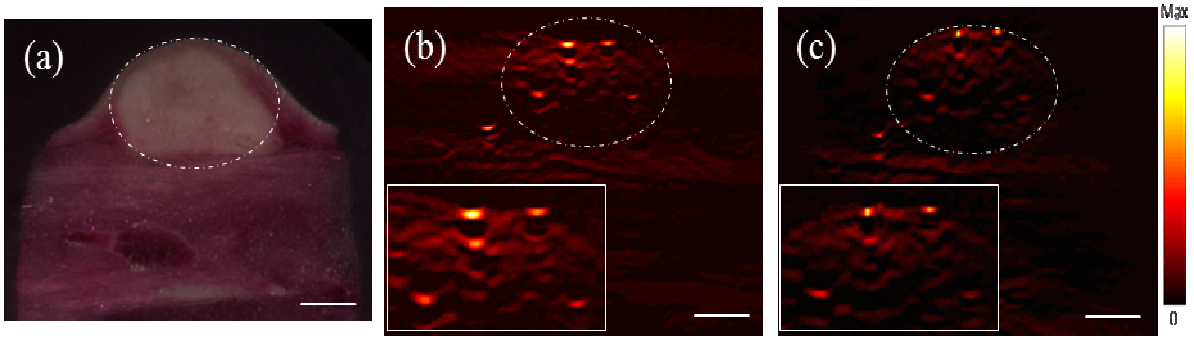

Fig. 4. (a) photograph of a cryoslice through a mouse containing the tumor or corresponding to the imaged cross-section. Reconstruction images in the linear (b) and curved (c) mode. The tumor is indicated with a dotted ellipse, and the curved detector allows for better tumor delineation and higher contrast to noise ratio compared to the linear scan which showcases higher background and lower overall resolution. The inserts depict a magnified in-scale view of a central vessel resolved in the tumor, indicated on (b) and (c) by the dash ellipse and demonstrate the resolution improvement in curved scanning. Scalebar 2 mm.

4. DISCUSSION AND CONCLUSION

In conclusion, we presented optoacoustic endoscopy based on the translation of a single ultrasound element in linear and curved geometries. We analyzed the image performance achieved by the two implementation using phantoms and ex-vivo tissue samples. The curved scanning geometry achieved better image quality than the linear scanning configuration. The resolution as characterized from the microsphere phantom has improved at least 27%. In the paper phantom, the shape structure of the circles and triangle obtained in the curved mode is more congruent with the reference image than in the linear scan. The reason for these improvements is that in optoacoustic imaging sources generated inside the region of interest radiate spherical waves in all directions. In a curved geometry, where detectors partially surround the region of interest, a larger portion of the acoustic field can be detected thus resulting in the detection of more complementary information and as a consequence better image quality. This makes the curved geometry particularly interesting for a detailed examination of lesions such as polyps or flat adenomas in colonoscopy. Conversely, the linear geometry offers a limited viewing angle which

reduces the image quality with respect to lateral resolution over the curved geometry. In the linear approach, the lateral resolution is proportional to the detector size $R_L(h) = \sigma$ [12], whereas in the curved geometry lateral resolution scales by $R_C(r) = (r / r_0)\sigma$ [12]. σ represents the diameter of the detector, r the position and r_0 the radius of the detection arc.

Image quality in both geometries could be further enhanced using a detector with a larger sensing angle. The IVUS detector utilized herein has a quite narrow field of view due to its shape and high central frequency. A transducer with a large aspect ratio (large in elevation and narrow in scanning direction) would satisfy such conditions, or alternatively the combination of a big detection element with a negatively focused lens. The implementation herein employed fixed illumination. This is advantageous from a tomographic reconstruction point of view, but has the limitation that a high power laser is necessary to illuminate the whole area of interest. In combination with high repetition rate lasers necessary to impart fast imaging performance, this might be problematic from a laser safety limit point of view. Future implementations will therefore scan the small illumination unit together with the detection unit and use lower energy lasers. The change of the acoustic field due to changing illumination conditions can be dealt with using model-based reconstruction algorithms [13]. Moreover, by adding additional rotation movement, the presented 2D imaging approach can be extended to 3D. Overall, the presented concept could be used together with optical endoscopes to yield hybrid optical and optoacoustic imaging performance better than the one be achieved by optical imaging alone. To enable passing the curved endoscope through the working channel of an optical endoscope one could employ a pre-shaped guidewire with a good shape memory or a guide-wire with an actively deflectable tip.

ACKNOWLEDGMENTS

The research leading to these results has received funding from the European Union project FAMOS (FP7 ICT, contract no. 317744).

REFERENCES

[1] R. Lambert, K. Kuznetsov, and J. F. Rey, "Narrow-band imaging in digestive endoscopy," *ScientificWorldJournal,* vol. 7, pp. 449-65, 2007.
[2] T. S. Kirtane and M. S. Wagh, "Endoscopic Optical Coherence Tomography (OCT): Advances in Gastrointestinal Imaging," *Gastroenterol Res Pract,* vol. 2014, p. 376367, 2014.
[3] A. Hoffman, M. Goetz, M. Vieth, P. R. Galle, M. F. Neurath, and R. Kiesslich, "Confocal laser endomicroscopy: technical status and current indications," *Endoscopy,* vol. 38, pp. 1275-83, Dec 2006.
[4] A. T. Committee, V. Kaul, D. G. Adler, J. D. Conway, F. A. Farraye, S. V. Kantsevoy*, et al.*, "Interventional EUS," *Gastrointest Endosc,* vol. 72, pp. 1-4, Jul 2010.
[5] J. M. Yang, C. Favazza, R. Chen, J. Yao, X. Cai, K. Maslov*, et al.*, "Simultaneous functional photoacoustic and ultrasonic endoscopy of internal organs in vivo," *Nat Med,* vol. 18, pp. 1297-1302, Aug 2012.
[6] D. Razansky, M. Distel, C. Vinegoni, R. Ma, N. Perrimon, R. W. Köster*, et al.*, "Multispectral opto-acoustic tomography of deep-seated fluorescent proteins in vivo," *Nature Photonics,* vol. 3, pp. 412-417, 2009.
[7] J. M. Yang, R. Chen, C. Favazza, J. Yao, C. Li, Z. Hu*, et al.*, "A 2.5-mm diameter probe for photoacoustic and ultrasonic endoscopy," *Opt Express,* vol. 20, pp. 23944-53, Oct 8 2012.
[8] J. M. Yang, K. Maslov, H. C. Yang, Q. Zhou, K. K. Shung, and L. V. Wang, "Photoacoustic endoscopy," *Opt Lett,* vol. 34, pp. 1591-3, May 15 2009.
[9] S. Sethuraman, S. R. Aglyamov, J. H. Amirian, R. W. Smalling, and S. Y. Emelianov, "Intravascular photoacoustic imaging using an IVUS imaging catheter," *Ieee Transactions on Ultrasonics Ferroelectrics and Frequency Control,* vol. 54, pp. 978-986, May 2007.
[10] H. He, A. Buehler, and V. Ntziachristos, "Optoacoustic endoscopy with curved scanning," *Opt Lett,* vol. 40, pp. 4667-70, Oct 15 2015.
[11] M. Xu and L. Wang, "Universal back-projection algorithm for photoacoustic computed tomography," *Physical Review E,* vol. 71, 2005.

[12] M. H. Xu and L. H. V. Wang, "Photoacoustic imaging in biomedicine," *Review of Scientific Instruments,* vol. 77, p. 041101, Apr 2006.
[13] T. Jetzfellner, A. Rosenthal, A. Buehler, A. Dima, K. H. Englmeier, V. Ntziachristos*, et al.*, "Optoacoustic tomography with varying illumination and non-uniform detection patterns," *J Opt Soc Am A Opt Image Sci Vis,* vol. 27, pp. 2488-95, Nov 1 2010.